Atmos. Chem. Phys. Discuss., 13, 26893–26931, 2013
www.atmos-chem-phys-discuss.net/13/26893/2013/
doi:10.5194/acpd-13-26893-2013

Atmospheric Chemistry and Physics Discussions

Uncertainties in future climate predictions due to convection parameterisations

H. Rybka and H. Tost

Institute for Atmospheric Physics, University of Mainz, Mainz, Germany

Received: 1 August 2013 – Accepted: 24 September 2013 – Published: 16 October 2013

Correspondence to: H. Rybka (rybkah@uni-mainz.de)

Published by Copernicus Publications on behalf of the European Geosciences Union.

Abstract

In the last decades several convection parameterisations have been developed to consider the impact of small-scale unresolved processes in Earth System Models associated with convective clouds. Global model simulations, which have been performed under current climate conditions with different convection schemes, significantly differ among each other in the simulated transport of trace gases and precipitation patterns due to the parameterisation assumptions and formulations, e.g. the simplified treatment of the cloud microphysics. Here we address sensitivity studies comparing four different convection schemes under alternative climate conditions (doubling of the CO_2 concentrations) to identify uncertainties related to convective processes. The increase in surface temperature reveals regional differences up to 4 K dependent on the chosen convection parameterisation. The increase in upper tropospheric temperature affects the amount of water vapour transported to the lower stratosphere. Furthermore, the change in transporting short-lived pollutants within the atmosphere is highly ambiguous for the lower and upper troposphere. Finally, cloud radiative effects have been analysed uncovering a shift in different cloud types in the tropics.

1 Introduction

Climate change due to increasing anthropogenic emissions is usually predicted with the help of Earth System Models (ESMs). Typically, the equilibrium climate sensitivity is specified as a measure of global mean temperature increase at the surface caused by a doubling of the carbon dioxide concentration (Cess et al., 1990). The change of the earth's temperature is a consequence of a changing heat budget of the atmosphere (and the ocean) accompanied by the redistribution of water vapour, the most important greenhouse gas, influencing the incoming and outgoing radiation. Both, heat and water vapour budgets are strongly coupled with atmospheric moist convection, which generally cannot be resolved directly in global atmospheric models. The pa-

ACPD
13, 26893–26931, 2013

rameterisation of convection, which represents small-scale cloud processes, induces much of the uncertainty concerning predictions of climate variability (Randall et al., 2003; Arakawa, 2004). In the last decades a variety of convection schemes have been developed (i.e., Arakawa and Schubert, 1974; Tiedtke, 1989; Hack, 1994; Zhang and McFarlane, 1995; Emanuel and Zivkovic-Rothman, 1999; Donner et al., 2001; Bechtold et al., 2001; Nober and Graf, 2005), some of them are slightly different, whereas most of them vary significantly in the description of convective processes. In principle, every scheme attempts to describe the statistical effect of moist convection to adjust the energy and water budget of the atmosphere into a more stable state.

Previous studies have compared different convection parameterisations in an ESM applying current climate conditions. The results indicate large differences in the simulated water vapour distribution and in the transport of short-lived trace gases due to a change of the convection scheme (Mahowald et al., 1997; Tost et al., 2006, 2010; Zhang et al., 2008). The region with the highest sensitivity is the upper troposphere-lower stratosphere (UTLS) in the intertropical convergence zone (ITCZ), which is dominated by the ascending vertical motion driven by convective cells. Therefore, it is anticipated that these uncertainties will propagate to alternate and future climate predictions. Another major source of uncertainty regarding model projections of global warming is the effect of clouds on the radiation budget (Stephens, 2005; Solomon et al., 2007). The huge spread of simulated cloud radiative feedbacks, occurring among climate models for more than a decade, has been observed in several studies (Cess et al., 1989; Colman, 2003; Soden and Held, 2006; Bony et al., 2006) and recognized as a key factor of the uncertainty in climate change since the 1970s (i.e., Charney, 1979). The complexity of this problem is attributed to cloud-induced flux changes (so called cloud radiative forcing; CRF) of the net shortwave and longwave radiation compared to clear-sky conditions. The modification of clouds on the radiative fluxes in the atmosphere is strongly dependent on the specific cloud type and can substantially vary in magnitude and sign (Chen et al., 2000; Hartmann et al., 1992, 2001). Areas which contribute the most to inter-model differences of simulated CRFs are regimes of moderate subsidence in

ACPD
13, 26893–26931, 2013

tropical regions reflecting low-level clouds in trade wind regions (Bony et al., 2004). These regimes are often closely related to deep convective cells, which influence regions of mean subsidence (Emanuel et al., 1994; Larson et al., 1999). Consequently, convection schemes alter cloud radiative forcing and its feedback.

Since, convection schemes interact with large-scale cloud parameterisations, which describe the process of condensation and evaporation on the grid scale, and consequently cloudiness and precipitation, their interdependency (subgrid scale ↔ large scale processes) influences total precipitation patterns and the amount and type of clouds, thus affecting cloud radiation properties (Hourdin et al., 2006).

Here we present an intercomparison of 16 simulations that differ with respect to the convection parameterisation, climatic distinction and model resolution. The focus is to identify and quantify uncertainties in simulated temperature increase, cloud radiative forcing and transport processes due to changes induced by the usage of different convection parameterisations. In order to avoid ambiguities, the term "sensitivity" is used in the sense of "sensitivity of cloud radiative feedbacks to convection parameterisation". These cloud radiative feedbacks certainly influence the sensitivity of the climate system (Colman, 2003; Ringer et al., 2006; Bony et al., 2006).

This study extends sensitivity studies of convection parameterisations which have been performed under current climate conditions (Tost et al., 2006, 2010). It was shown, that an exchange of the convection parameterisation significantly modifies the water vapour and temperature distribution in the UTLS region, especially in low latitudes. Furthermore, discrepancies in precipitation patterns and cloudiness have been found to alter the radiation and energy budget of the atmosphere. This work focuses on the impact of different convection schemes influencing meteorological variables under climate change conditions.

In Sect. 2 an overview of the model and simulation setup is given. Section 3 concerns with mathematical methods, which are used to interpret the results in Sect. 4. The results are divided into several subsections dealing with differences in the temperature

ACPD
13, 26893–26931, 2013

distribution, precipitation, transport of short-lived trace gases and the cloud radiative forcing. Our conclusions are given in Sect. 5.

2 Model description and simulation setup

2.1 Model description

To analyse the impact of convection parameterisations the ECHAM5/MESSy atmospheric chemistry model (EMAC, Joeckel et al., 2010) is used. It is a combination of the 5th generation of the European Centre Hamburg general circulation model (ECHAM5, Roeckner et al., 2006) and the Modular Earth Submodel System (MESSy, Joeckel et al., 2005). The former calculates the atmospheric flow with the prognostic variables (vorticity, divergence, temperature, total moisture and the logarithm of the surface pressure) and is integrated in the Base Model Layer of MESSy (Joeckel et al., 2005). The interface structure of MESSy allows to use different submodels linking modules for atmospheric chemistry, transport or diagnostic tools with the meteorology. The modularization implies an equivalent configuration for every simulation, distinguishing only by the chosen convection parameterisation in the submodel CONVECT and the carbon dioxide concentration of the atmosphere used in the radiation calculations (submodel RAD4ALL). The implementation of atmospheric chemistry processes is neglected, as well as the simulation of the ocean circulation. The latter consequently determines the requirement of boundary conditions (e.g. sea surface temperatures and sea ice content) for the simulations.

2.2 Simulation setup

For this study two scenarios are calculated with EMAC (Roeckner et al., 2006; Joeckel et al., 2005, 2010), applying each four different convection schemes (see Table 1). Additional information about the individual convection parameterisations and their implementation are described in Tost et al. (2006) and references therein. Each set of

ACPD
13, 26893–26931, 2013

experiments includes a reference simulation (hereafter referred to as REF) with a carbon dioxide concentration of 348 ppm and a double CO_2-simulation (abbr. $2 \times CO_2$) with a CO_2 concentration of 696 ppm. Oceanic boundary conditions are prescribed with external data. For this purpose, climatological monthly average sea surface temperatures (SST) and sea ice contents (SIC) from 1987 to 2006 from the AMIP database are used for the reference simulation. Concerning the $2 \times CO_2$-simulation, data of a coupled atmosphere–ocean general circulation model (increased/decreased SSTs/SICs), which has been run under similar climate conditions (CO_2 concentration of 696 ppm), have been used to maintain the radiative equilibrium (M. Ponater, personal communication, 2012). Two horizontal resolutions (T42 and T63) are applied with 31 vertical hybrid pressure levels up to 10 hPa for each simulation, which results in 16 simulations spanning up a space of the chosen convection parameterisation, resolution and climate condition.

The simulation period spans 10 yr, considering the first year of the simulation as spin-up and therefore discarding it from the analysis in each case. Monthly averaged output data have been used for the analysis. It should be mentioned that because of the coarse vertical resolution for the stratosphere, circulation patterns in these altitudes are insufficiently resolved. Therefore, results for these regions should be treated carefully.

3 Methods

The variety of simulations allows many possibilities for comparisons, therefore a consistent notation is required to avoid possible confusion. To compare a variable x of two (or more) simulations the following notations are used:
The symbol Δ indicates the difference between the $2 \times CO_2$- and REF-simulation considering the same convection scheme (i = T1, EC, EM or ZM) in both runs, i.e.:

$$\Delta x_i = x_{i,2\times CO_2} - x_{i,\mathrm{REF}} \quad (1)$$

ACPD
13, 26893–26931, 2013

To identify the differences between two individual simulations with the same CO_2 concentration the character δ and subscripts distinguishing the convection schemes are applied. For example, the difference of a variable x between the REF-simulations of EM and T1 is calculated as follows:

$$\delta^{\mathrm{EM}}_{\mathrm{T1}} x_{\mathrm{REF}} = x_{\mathrm{EM,\,REF}} - x_{\mathrm{T1,\,REF}} \tag{2}$$

The combination of Eqs. (1) and (2) results in:

$$\begin{aligned}\delta^{\mathrm{EM}}_{\mathrm{T1}}(\Delta x) &= \Delta x_{\mathrm{EM}} - \Delta x_{\mathrm{T1}} \\ &= (x_{\mathrm{EM,\,2\times CO_2}} - x_{\mathrm{EM,\,REF}}) - (x_{\mathrm{T1,\,2\times CO_2}} - x_{\mathrm{T1,\,REF}}),\end{aligned} \tag{3}$$

where $\delta^{i}_{j}(\Delta x)$ represents the uncertainty of a changing quantity x between two convection schemes (whereas $i,j =$ T1, EC, EM or ZM and $i \neq j$). Finally, a measure is needed to compute the maximum error or variability of a variable due to a change of the convection parameterisation for one resolution.

$$x_{\mathrm{Var}} = x_{\mathrm{max}} - x_{\mathrm{min}}, \tag{4}$$

where $x_{\mathrm{max}} = \mathrm{MAX}(x_{\mathrm{T1}}, x_{\mathrm{EC}}, x_{\mathrm{EM}}, x_{\mathrm{ZM}})$,

and $x_{\mathrm{min}} = \mathrm{MIN}(x_{\mathrm{T1}}, x_{\mathrm{EC}}, x_{\mathrm{EM}}, x_{\mathrm{ZM}})$.

Equation (4) displays the maximum error by selecting the minimum value x_{min} of four simulations at a specific grid point (and/or level) and subtracting it from the corresponding maximum value x_{max} at the same location.

For the following section, one has to keep in mind that the analysed variables are 9 yr averaged values of the monthly output data.

ACPD
13, 26893–26931, 2013

4 Results

4.1 Temperature

As convection influences the atmospheric heat budget and consequently the temperature profile (Yanai et al., 1973; Johnson, 1984), differences in the temperature profiles of the REF- and 2 × CO_2-simulations are analysed.

Figure 1 shows the simulated global mean temperature increase/decrease (ΔT) in the troposphere/stratosphere due to a doubling of the carbon dioxide concentration and the application of different convection parameterisations and model resolutions.

Qualitatively, the general characteristics of the vertical temperature change profile are independent of the selected resolution and convection scheme: a gradual increase from 3 to 5 K up to 300 hPa accompanied by a gain in radiative energy which is not uniformly distributed within the troposphere because of advection and convective mixing. In contrast, the stratospheric temperature decrease is related to enhanced absorption and re-emission of higher CO_2 concentrations. The differences between individual simulations are on average below 0.5 K, but show significant variations around 600 hPa and above 400 hPa. These two regions of high model to model fluctuations are related to two mechanisms associated with different formalisms in the convection schemes. Firstly, the representation of microphysics strongly influences the formation of precipitation as well as ice and snow formation and is therefore connected to the release and/or need of energy for phase transformations, especially around 600 hPa. Secondly, the transport of water vapour by convective updrafts to high altitudes affects the radiation, thereby altering the temperature above 400 hPa. These two processes are the major reasons for the variability in the temperature change between the individual simulations. The comparison of Fig. 1a and b reveals no obvious differences for ΔT induced by a change of the model resolution. Figure 2 presents a correlation of the temperature change between the resolution T63 and T42. The individual simulations are distinguished by various symbols and colour coded with pressure altitude. Figure 2 shows that the correlation between the two resolutions is very high ($R^2 \geq 0.9976$) and

ACPD
13, 26893–26931, 2013

the linear regression is close to the one-to-one line, particularly below 400 hPa (red to yellow symbols). Nevertheless, a tendency of higher temperature changes ΔT for the resolution T63 is evident in every simulation for pressure altitudes between 50 hPa and 300 hPa.

Table 2 compares the simulated temperature increase for the lowermost model layer and their biases compared to the reference simulation T1. The globally averaged values for ΔT lie within a range of 3.3 to 3.5 K without significant differences among the resolutions. The EC simulation produces a slightly higher temperature increase compared to the other simulations. Apparently, most of the global mean temperature increase is strongly restricted to the prescribed boundary conditions for the $2 \times CO_2$-simulation over the oceans, but reveals higher regional variations over the land surface. Figure 3 shows this variability by displaying the maximum error ΔT_{Var} (see Eq. 4) of the temperature increase ΔT for either the lowermost model layer and the zonal mean induced by a change of the convection parameterisation. This variable helps to identify regions on the globe and within the atmosphere, which show a high sensitivity to a change of the convection scheme. In Fig. 3 these regions are explicitly illustrated by green, yellow and brown colours highlighting variations of ΔT above 1.0 K. These regions encompass the ITCZ in Africa and South America displayed in Fig. 3a and b as well as areas north and south of 60°. The latter specifies zones which vary significantly in snow and ice cover over land between the simulations. Strong variations in high latitudes result from interactions between the boundary layer (parameterisation), the boundary condition and the convection scheme, whereas the variability for the ITCZ region is exclusively determined by the diverse simulation of convection. The most notable feature is visible over the continents Africa and South America, ΔT_{Var} is approximately ΔT_{min} (black contour lines in Fig. 3), which means that the change of the convection parameterisation produces a range of the average temperature increase in these regions between 2 K and 6 K. Consequently, the impact using a different convection scheme according the temperature change is large in the ITCZ but negligible with respect to global mean values (see Table 2). The comparison of the resolutions in Fig. 3a and b provide evidence

ACPD
13, 26893–26931, 2013

for lower model-to-model fluctuations of the sensitivity in local surface temperature response to convective changes over Africa for the horizontal resolution T63. This indicates that the relative importance of the convection schemes decreases with higher model resolution due to the ability to partly resolve atmospheric phenomena better. Regarding the zonal mean distribution of ΔT_{Var}, larger values are located in the UTLS and around 600 hPa in the ITCZ (see Fig. 3c and d), pronouncing the temperature variability for these pressure heights shown in Fig. 1. But besides that, a higher variability is also visible around 70° N and 80° S, which indicate regions with a large change in snow and ice cover. This result points out that differences in the interaction between convection schemes and the boundary layer influence the whole temperature profile of the troposphere, which for this case is also determined by a change of convective triggering (see Sect. 4.2).

4.2 Trigger function/mechanism

During the simulation the calculation process of the convection scheme is repeated every time step, while the first decision in every cycle defines one grid cell as convective or non-convective. This determination is done by the so called "trigger" function by examining if the actual atmospheric environment favours the convective ascent of an air parcel or suppress its rise. Each convection parameterisation uses a different kind of trigger mechanism, consequently altering the occurrence of convection as well as the type (shallow, midlevel or deep). A change in this small part of the parameterisation could affect the model climate (Jakob and Siebesma, 2003). The most common trigger function adds a virtual temperature excess (typically 0.5 to 1 K) to the buoyant air parcel to overcome a potential barrier at cloud base (relevant for T1, EM and ZM). Another approach for the trigger mechanism, which is pursued by the ECMWF scheme, is the criterion regarding a positive vertical velocity for the air parcel at cloud base (Tompkins et al., 2004). These criteria determine the trigger function and the overall appearance of convection. The zonal activation of convection for the reference simulations is displayed in Fig. 4a and b. Each bar represents an average activation over

ACPD
13, 26893–26931, 2013

30° latitude for the overall (deep) convection of one reference simulation displayed by the filled (hatched) bar height. Independent of the resolution, large differences occur among the simulations, in particular for the T1 and EC simulations. Whereas the EM and ZM simulation produce similar results, the Tiedtke scheme shows a completely different distribution for the deep convective clouds with higher values for high latitude regions. This can be explained by the additional activation of midlevel convection which is not implemented in the EM and ZM-schemes. Nevertheless, the overall activation of T1 is comparable with the EM and ZM simulations. Although the ECMWF scheme considers midlevel convection, significantly lower values for the activtity of total and deep convection are obtained. The distribution for the EC simulation demonstrates that another trigger criterion could lead to a completely different convection occurrence independent of the applied resolution. The bottom row of Fig. 4 displays the relative change of the convection activation for the $2 \times CO_2$-simulation. Again, the height of the filled (hatched) bars illustrate the relative change of all (deep) convective events. The largest shift in the activation of the convection scheme is located at the poleward regions in both hemispheres. Changes of ±10 % concerning all convective events and changes up to ±50 % for deep convective events are evident dependent on the selected convection parameterisation. The decrease of the sea ice content and the stronger increase in moisture and temperature in the polar regions leads to more triggering of deep convective events in the $2 \times CO_2$-simulation. The highly variable change of the activation between the individual simulations for the polar regions explains the temperature variability in Fig. 3. Regarding the latitudinal band between 60° S and 60° N, the T1 simulation features a reduced activation of deep convective events. On the contrary, no significant changes are evident for the EC, EM and ZM simulation in these regions.

4.3 Transport of humidity and short-lived trace gases

The analysis of the vertical transport of water vapour and other trace gases reveals high differences between the convection parameterisations. Previous studies quantified that the uncertainty in the concentrations of simulated trace gases due to a change of the

ACPD
13, 26893–26931, 2013

convection scheme could locally exceed 100 % (Tost et al., 2010; Zhang et al., 2008). Atmospheric convection modifies the distribution of chemical tracers and water vapour by lifting boundary layer air to middle or upper tropospheric levels. Investigating the increase in specific humidity q (Fig. 5), similar characteristics compared to the temperature increase (Fig. 2) can be identified. The inner panel of Fig. 5 shows the global mean increase of specific humidity Δq in % for the resolution T42 indicating a strong increase of up to 90 % at 150 hPa. At the same time, this region depicts the largest variability of increasing water vapour between the simulations. The comparison between the resolution dependent increase of the specific humidity in Fig. 5 reveals different aspects. A high correlation is clearly visible up to 400 hPa close to the one-to-one line, as well as a larger spread for the UTLS region for each respective convection scheme. Having a closer look at the increase in specific humidity above 100 hPa (purple coloured symbols), a higher increase for the coarser resolution is shown, indicating a higher transmittance of the tropopause layer for transport processes in the resolution T42. In contrast, the T63 simulations point out a significantly higher increase in water vapour between 100 hPa and 300 hPa. This result demonstrates that the tropopause operates as a stronger transport barrier for convection in simulations with higher resolutions. Especially, the EM-simulation shows a lower relative increase in specific humidity for the resolution T42 up to 100 hPa. The high variability of increasing specific humidity for the various simulations in the upper troposphere is consistent with a previous study, which shows strong differences in the simulated water vapour content of the UTLS region dependent on the chosen convection parameterisation (Tost et al., 2006). Therefore, it is hardly surprising that the change in specific humidity is strongly influenced by the applied convection scheme under a doubling of the CO_2 concentration.

Another way to identify the change of vertical transport in the atmosphere is to analyse short-lived trace gases. A typical tracer to investigate convective transport is radon (^{222}Rn) (Allen et al., 1996; Mahowald et al., 1997; Dentener et al., 1999; Zhang et al., 2008). This chemically inert trace gas is emitted from soil and decays radioactively with a half-life of 3.8 days to lead (^{210}Pb) which simultaneously represents the only sink. To

ACPD
13, 26893–26931, 2013

simulate the transport of radon a common assumption is a constant emission rate of 1 atom $(cm^2\,s)^{-1}$ over (ice and snow free) land and zero over sea (Turekian et al., 1977; Jacob et al., 1997; Rasch et al., 2000). It has to be kept in mind, that this assumption leads to vertical radon profiles which represent to a great extent the convective transport over continental areas and not over oceans. A strict comparison of the vertical radon distribution between the convection schemes requires equal emissions of radon for each simulation. This condition is not satisfied, because the ice and snow cover over land varies in time and place. Therefore, zonally averaged radon ratios are computed which are scaled to the total atmospheric radon column mass for the respective simulation. This approach allows a universal comparison independent of the absolute radon emission. Figure 6 shows the zonal average vertical distribution of radon for 30° latitude bands displaying the radon ratio for the REF-simulation T1. The distribution of the EC-, EM- and ZM-simulations are illustrated by relative differences compared to the T1-simulations. A typical zonal distribution of the absolute radon mass (or mixing ratios) has maximum values at ground levels and shows a decrease with increasing height, because of the short residence time (not shown). Looking at the radon ratios in Fig. 6 the maxima are located around 900 hPa and reduced values for lower pressure levels are visible independent of the latitude band. Within the boundary layer, small radon ratios are calculated because of the comparatively small vertical extent for near ground levels and thus lower grid box masses. The highest ratios are simulated for the Northern Hemisphere reflecting the larger zonal land amount and associated emissions in these latitudes. Only small differences between the convection schemes are apparent in the lower altitudes of the mid-latitudes. In the ITCZ region significant variations ranging from −40 % for the lower troposphere up to above 100 % in the UTLS region are evident. The variability of the radon ratios in the tropics confirm that simulating fast transport is strongly influenced by the convection scheme. The relative change of radon due to an increase of carbon dioxide is illustrated in Fig. 7. Regarding the mid-latitudes and polar regions each convection scheme shows an increase of the radon ratio below 700 hPa of 10 % and a decrease of −25 % above this pressure alti-

ACPD
13, 26893–26931, 2013

tude indicating a weaker vertical transport. This is in agreement with a decrease of the upward massflux because of a higher stability (lower vertical temperature gradient) of a warmer climate. In the ITCZ region a reduction of radon ratios between 200 hPa and 400 hPa is simulated and a strong increase above 200 hPa distinguishing a weaker but higher ascent of radon due to a shift of the tropopause (see black dashed and solid line). The distribution below 400 hPa in the tropics is widely different among the experiments changing the convection schemes. Whereas the EC and ZM simulations simulate higher radon ratios of up to 10 %, the others display only minor changes. Apparently, the choice of the convection parameterisation strongly alters the transport of boundary layer air to the free troposphere in the 2 × CO_2-scenario.

4.4 Cloud radiative forcing and cloud types

One major concern in the community of climate modellers is the correct representation of cloud radiative effects. This has been discussed for several years and is stated as the largest source of uncertainty estimating climate sensitivity (Bony et al., 2006; Soden and Held, 2006). Many physical processes related to cloud formation take place on scales which are smaller than usual ESM resolutions and therefore have to be parameterised. For example, subgrid-scale structures of clouds reflecting inhomogeneities of cloud liquid and ice contents can influence radiative fluxes and precipitation rates which are not (or only barely) considered in ESMs (Barker and Raisanen, 2005). The purpose of this section is to identify the strength of interaction between the cloud and convection schemes by examining the change in cloud types and cloud radiative forcing (CRF). We assume that the redistribution of moist air through the different entrainment and detrainment rates parameterised in diverse approaches in the convection schemes produces various cloud types and hence a diverse cloud radiative feedback under alternative climate conditions. To identify the differences of cloud-induced radiative flux changes the following calculations have been performed:

The global mean cloud radiative forcing describes the difference between the all-sky

ACPD
13, 26893–26931, 2013

and clear-sky radiative fluxes:

$$\mathrm{CRF} = F - F_{\mathrm{clr}} \tag{5}$$

where F_{clr} describes the total net radiative flux at the top of the atmosphere (TOA) under clear-sky conditions and F with the same meaning for all-sky conditions. On a global average Eq. (5) produces a negative value for the CRF, revealing that clouds cool the entire Earth system. Furthermore, one could characterise the magnitude of the CRF by separating the amount into a longwave (LW) and shortwave (SW) component:

$$\mathrm{CRF} = \mathrm{CRF}_{\mathrm{SW}} + \mathrm{CRF}_{\mathrm{LW}} \tag{6}$$

where $\mathrm{CRF}_{\mathrm{SW}}$ (< 0) and $\mathrm{CRF}_{\mathrm{LW}}$ (> 0) are calculated equally to Eq. (5) for the shortwave and longwave net radiative fluxes, respectively. The negative sign for the shortwave component results because of the higher reflectivity of clouds with regard to the surface. The positive sign concerning the longwave component characterises the lower emission temperature of clouds with respect to the surface. Therefore it is obvious, that the magnitude of these two components is highly variable for different cloud types (Hartmann et al., 1992).

The change in cloud radiative forcing (ΔCRF; also known as cloud radiative feedback) is computed according to Eq. (1) and global mean values are listed in Table 3.

In order to explain these results the fundamental causes which produce the change in cloud radiative forcing have to be analysed. These are (neglecting the change in surface albedo, which is nearly the same in every REF- and $2 \times CO_2$-simulation):

a. change in cloud cover

b. changes of different cloud types
(reflecting alterations in cloud top height and optical thickness)

According to (a), the globally averaged cloud cover for the REF-simulations vary between 58 to 63 % (not shown). The change in cloud cover is similar in every $2 \times CO_2$-simulation with a reduction of 2 to 2.5 % inducing a net positive cloud radiative feedback

ACPD
13, 26893–26931, 2013

in consistency with Table 3. Nevertheless, the changes in short- and longwave CRF components primarily reveal a highly variable change in cloud types dependent on the convection scheme. To illustrate this, cloud types defined by the International Satellite Cloud Climatology Project (ISCCP) (Rossow and Schiffer, 1999) are calculated online in the model via the ISCCP simulator (Klein and Jakob, 1999; Webb et al., 2001), which categorizes cloud types based on their cloud top pressure (p_c) and optical depth (τ). Zonal cloud type distributions for the REF-simulations are shown in Fig. 8 (including very thin clouds with $\tau < 0.3$). First of all, it should be mentioned that a comparison with the ISCCP D1 dataset (multi-year average values of 1984 until 2008 for the selected cloud types) reveals a strong overestimation of tropical cirrus (partly induced by non-observed very thin cloud structures i.e. subvisible cirrus in the ISCCP data) as well as optically thick clouds ($\tau > 23 \Rightarrow$ Stratus, Nimbostratus and Deep Convective) in all simulations. Cumulus, Altocumulus and Altostratus are hardly simulated and therefore underestimated compared to the ISCCP data, in agreement with the findings of Zhang et al. (2005) and Raisanen and Jarvinen (2010). Nevertheless, these errors compensate in such a way, that radiative equilibrium is achieved and global mean CRF values lie in a reasonable range between -17 and $-27\,\mathrm{W\,m^{-2}}$ for the reference simulations. Despite that, focusing on the variability of cloud types due to a change of the convection parameterisation, Fig. 8 displays significant variations for thick clouds as well as Stratocumulus over all latitudes. The variability easily exceeds 10 % for most cloud types compared with its mean value over all simulations in one zonal region. The change in cloud types is far smaller comparing the different resolutions than an exchange of the convection scheme. Consequently, it is important to take into account that convection parameterisations could have a significant influence on the cloud fraction by interacting with the large-scale cloud scheme, as supposed by Raisanen and Jarvinen (2010).

The absolute and relative change in cloud type amount for three 60° latitudinal bands of the $2 \times CO_2$-simulations is displayed in Fig. 9, whereas only the two highest (positive and negative) changes are explicitly labelled. At northern and southern mid-latitudes, an increase of deep convective as well as cirrostratus or cirrus clouds of ~ 25 % is vis-

ACPD
13, 26893–26931, 2013

ible. In contrast, Nimbostratus, Stratocumulus and Altostratus clouds are diminished to a greater extent comparing the absolute change in the same region, therefore inducing a positive cloud radiative feedback for all simulations (cf. Table 3). The differences between the different simulations for these latitudes are small compared to the tropics. Consequently, the diverse magnitude of ΔCRF is primarily caused by high variations of tropical cloud type changes, which is analysed further. In the case of the EC simulation a strong increase of deep convective and cirrostratus clouds compensate the reduction of cirrus clouds inducing a positive change for ΔCRF_{LW}, a small reduction of the shortwave CRF component and accordingly a minor positive cloud radiative feedback for the T42 resolution. Around the equator more deep convective cells are simulated with the convection parameterisation of Zhang–McFarlane–Hack, however a decrease of the longwave CRF component illustrates that cloud top heights are not significantly increasing because of the higher stability of the warmer atmosphere. The T1 and EM simulations show no changes for convective clouds in the tropics, only a reduction in cirrus clouds, an effect which is most prominent when using the Emanuel convection scheme entailing a strong positive shortwave cloud feedback. The T63 simulations result in similar changes compared to the T42 resolution for the T1, EM and ZM schemes for ΔCRF_{LW} but smaller values for the shortwave component, because of overall less changes in all cloud types and cloud cover compared to the REF-simulations resulting in a smaller cloud radiative feedback. The ECMWF scheme reacts differently displaying a higher shortwave cloud feedback and a negative longwave cloud feedback compared to the coarser resolution. Principally, a stronger reduction in cirrus clouds and a smaller increase of deep convective and cirrostratus clouds in the tropics is the reason of this shift in ΔCRF_{LW}.

Generally, the longwave cloud feedback is negative for all simulations (except EC T42). This feature does not confirm the fixed anvil temperature (FAT) hypothesis (Hartmann and Larson, 2002) but instead shows that a warmer climate could produce clouds with a proportionately higher anvil temperature (PHAT) (Zelinka and Hartmann, 2010) inducing a negative longwave cloud feedback. One possible explanation is the strong

ACPD
13, 26893–26931, 2013

increase in upper tropospheric temperature (~ 4.5 K) in comparison with the mean temperature change of 3.4 K reflecting a higher increase in cloud top temperature (not shown) than the increase of surface temperature.

It should be noted that the choice of the cloud scheme alters the variability of cloud type changes in a similar way. In this study the large-scale processes of condensation (cloud and precipitation formation) are based on work of Lohmann and Roeckner (1996) and Tompkins (2002). The sensitivity of other convection parameterisations on different cloud schemes is unknown and has not yet been investigated. This aspect remains unanswered but prompts speculations that other cloud schemes show similar variations by changing the convection parameterisation.

5 Conclusions

One major goal of this study was to investigate the range of uncertainty caused by a change of the convection parameterisation under warmer climate conditions. In total, 16 simulations have been performed with the EMAC model varying the CO_2 concentrations (348 ppm = reference run; 696 ppm = 2 × CO_2 scenario), resolution (T42; T63) and the convection schemes (Tiedtke, ECMWF, Emanuel and Zhang–McFarlane–Hack). The analysis shows significant influences on the temperature and humidity distribution, as well as the transport of short-lived trace gases and the cloud radiative feedback.

The variability of the global mean temperature change with respect to the vertical profile reveals differences up to 0.5 K in the middle and upper troposphere. The sensitivity in the mid-troposphere originates most likely from different formulations of the microphysics in the convection parameterisations, especially the treatment of snow and ice formation. Another important contribution is the diversity in the simulated transport of water vapour to the UTLS, which yields a higher uncertainty for the upper troposphere concerning the temperature change. The comparison of the global mean change in surface temperature shows very small differences. Nevertheless, regional variations cover a range from 2 to 6 K in tropical regions. This implies that the uncertainty of regional

ACPD
13, 26893–26931, 2013

temperature changes induced by a global warming can easily exceed 4 K comparing Earth System Models with different convection parameterisations.

Apart from influencing the temperature profile, transport mechanisms are affected by the chosen convection scheme. In consideration of a changing water vapour content in a $2 \times CO_2$ scenario the simulations with coarser resolutions prove that the tropopause is of higher transmittance comparing to the T63 simulations. Hence, a stronger increase in water vapour is visible in the lower stratosphere for the T42 simulations independent of the convection scheme. Furthermore, the analysis of the short-lived trace gas Radon verifies that a more stable state of the troposphere in the $2 \times CO_2$ scenario induces lower upward massfluxes and consequently a decreased transport of Radon up to 200 hPa in the ITCZ region. Additionally, the shift of the tropopause to higher altitudes superimposes the effect of a decrease in massfluxes and results in higher radon concentrations for the UTLS region. The largest differences according to the change in transport of Radon are visible in the lower troposphere ranging from −20 % to +20 % for the tropics. This uncertainty indicates that the different temperature increases over the continents in the ITCZ lead to distinctive initiation of convective transport from the boundary layer dependent on the selected convection parameterisation. Furthermore, the interaction of the boundary layer parameterisation and the convection scheme is sensitive concerning the strength of the calculated upward base massflux.

In connection with cloud formation their radiative effects have been analysed for all simulations. The cloud radiative feedback has been calculated revealing differences between the simulations of up to $1.7\,W\,m^{-2}$. The most important implication is the indirect interaction between cloud and convection schemes resulting in completely different cloud type changes for the tropics. This high variability of different changes in cloud types induces large differences in cloud radiative feedback and uncover a new source of uncertainty relating to convection parameterisations. The range of ΔCRF could point out a relevant indication for different climate sensitivities in coupled atmosphere–ocean GCMs induced by several convection schemes.

ACPD
13, 26893–26931, 2013

Model intercomparisons often contain different formulations for parametrising convection. Some uncertainties in these comparisons could be directly addressed to the difference in the convection scheme. This study shows that some uncertainties of future climate predictions are linked to the chosen representation of convective clouds as well and should be taken into account when comparing different models. It should be pointed out, that the results presented here are constrained to the fixed boundary conditions. To acquire a more consistent framework for future studies a coupled atmosphere–ocean GCM should be considered to achieve alternative climate conditions through transient simulations with increasing carbon dioxide concentrations for each convection scheme. These simulations would provide benefits to analyse the change in maritime convection and transport mechanisms over oceans via methyl iodide concentrations (Donner et al., 2007). Moreover, it is important to minimize the uncertainties presented here. A step forward could be to compare these results with simulations including a superparameterisation (Khairoutdinov et al., 2005) for near explicit representation of cloud processes considering subgrid-scale mechanisms through a cloud resolving model. An advantage of these multiscale models is a better account for low cloud fraction (Wyant et al., 2006) and the interaction between clouds and radiation at unresolved scales (Cole et al., 2005) which seems to be a dominant factor of high uncertainties in the net cloud radiative forcing.

Acknowledgements. We are grateful to M. Ponater for providing data of sea surface temperatures and sea ice contents for the $2 \times CO_2$ simulations and useful discussions. Furthermore, we wish to acknowledge use of the Ferret program for analysis and graphics in this paper. Ferret is a product of NOAAs Pacific Marine Environmental Laboratory. (Information is available at http://ferret.pmel.noaa.gov/Ferret/.) We would like to acknowledge high-performance computing support provided by the computing facilities at the Johannes Gutenberg-University and all MESSy developers for support and discussions.

ACPD
13, 26893–26931, 2013

References

Allen, D. J., Rood, R. B., Thompson, A. M., and Hudson, R. D.: Three-dimensional radon 222 calculations using assimilated meteorological data and a convective mixing algorithm, J. Geophys. Res.-Atmos., 101, 6871–6881, doi:10.1029/95JD03408, 1996. 26904

Arakawa, A.: The cumulus parameterization problem: past, present, and future, J. Climate, 17, 2493–2525, doi:10.1175/1520-0442(2004)017<2493:RATCPP>2.0.CO;2, 2004. 26895

Arakawa, A. and Schubert, W. H.: Interaction of a cumulus cloud ensemble with large-scale environment 1, J. Atmos. Sci., 31, 674–701, doi:10.1175/1520-0469(1974)031<0674:IOACCE>2.0.CO;2, 1974. 26895

Barker, H. W. and Raisanen, P.: Radiative sensitivities for cloud structural properties that are unresolved by conventional GCMs, Q. J. Roy. Meteor. Soc., 131, 3103–3122, doi:10.1256/qj.04.174, 2005. 26906

Bechtold, P., Bazile, E., Guichard, F., Mascart, P., and Richard, E.: A mass-flux convection scheme for regional and global models, Q. J. Roy. Meteor. Soc., 127, 869–886, doi:10.1256/smsqj.57308, 2001. 26895

Bechtold, P., Chaboureau, J. P., Beljaars, A., Betts, A. K., Kohler, M., Miller, M., and Redelsperger, J. L.: The simulation of the diurnal cycle of convective precipitation over land in a global model, Q. J. Roy. Meteor. Soc., 130, 3119–3137, doi:10.1256/qj.03.103, 2004. 26920

Bony, S., Dufresne, J. L., Le Treut, H., Morcrette, J. J., and Senior, C.: On dynamic and thermodynamic components of cloud changes, Clim. Dynam., 22, 71–86, doi:10.1007/s00382-003-0369-6, 2004. 26896

Bony, S., Colman, R., Kattsov, V. M., Allan, R. P., Bretherton, C. S., Dufresne, J. L., Hall, A., Hallegatte, S., Holland, M. M., Ingram, W., Randall, D. A., Soden, B. J., Tselioudis, G., and Webb, M. J.: How well do we understand and evaluate climate change feedback processes?, J. Climate, 19, 3445–3482, doi:10.1175/JCLI3819.1, 2006. 26895, 26896, 26906

Cess, R. D., Potter, G. L., Blanchet, J. P., Boer, G. J., Ghan, S. J., Kiehl, J. T., Letreut, H., Li, Z. X., Liang, X. Z., Mitchel, J. F. B., Morcrette, J. J., Randall, D. A., Riches, M. R., Roeckner, E., Schlese, U., Slingo, A., Taylor, K. E., Washington, W. M., Wetherald, R. T., and Yagai, I.: Interpretation of cloud-climate feedback as produced by 14 atmospheric general-circulation models, Science, 245, 513–516, doi:10.1126/science.245.4917.513, 1989. 26895

ACPD
13, 26893–26931, 2013

Cess, R. D., Potter, G. L., Blanchet, J. P., Boer, G. J., Del Genio, A. D., Deque, M., Dymnikov, V., Galin, V., Gates, W. L., Ghan, S. J., Kiehl, J. T., Lacis, A. A., Le Treut, H., Li, Z. X., Liang, X. Z., McAvaney, B. J., Meleshko, V. P., Mitchel, J. F. B., Morcrette, J. J., Randall, D., Rikus, L., Roeckner, E., Royer, J. F., Schlese, U., Sheinin, D. A., Slingo, A., Sokolov, A. P., Taylor, K. E., Washington, W. M., Wetherald, R. T., Yagai, I., and Zhang, M. H.: Intercomparison and interpretation of climate feedback processes in 19 atmospheric general-circulation models, J. Geophys. Res.-Atmos., 95, 16601–16615, doi:10.1029/JD095iD10p16601, 1990. 26894

Charney, J. G.: Carbon Dioxide and Climate: a Scientific Assessment, The National Academies Press, 1979. 26895

Chen, T., Rossow, W. B., and Zhang, Y. C.: Radiative effects of cloud-type variations, J. Climate, 13, 264–286, doi:10.1175/1520-0442(2000)013<0264:REOCTV>2.0.CO;2, 2000. 26895

Cole, J. N. S., Barker, H. W., Randall, D. A., Khairoutdinov, M. F., and Clothiaux, E. E.: Global consequences of interactions between clouds and radiation at scales unresolved by global climate models, Geophys. Res. Lett., 32, L06703, doi:10.1029/2004GL020945, 2005. 26912

Colman, R.: A comparison of climate feedbacks in general circulation models, Clim. Dynam., 20, 865–873, doi:10.1007/s00382-003-0310-z, 2003. 26895, 26896

Dentener, F., Feichter, J., and Jeuken, A.: Simulation of the transport of Rn-222 using online and off-line global models at different horizontal resolutions: a detailed comparison with measurements, Tellus B, 51, 573–602, doi:10.1034/j.1600-0889.1999.t01-2-00001.x, 1999. 26904

Donner, L. J., Seman, C. J., Hemler, R. S., and Fan, S. M.: A cumulus parameterization including mass fluxes, convective vertical velocities, and mesoscale effects: thermodynamic and hydrological aspects in a general circulation model, J. Climate, 14, 3444–3463, doi:10.1175/1520-0442(2001)014<3444:ACPIMF>2.0.CO;2, 2001. 26895

Donner, L. J., Horowitz, L. W., Fiore, A. M., Seman, C. J., Blake, D. R., and Blake, N. J.: Transport of radon-222 and methyl iodide by deep convection in the GFDL Global Atmospheric Model AM2, J. Geophys. Res.-Atmos., 112, D17303, doi:10.1029/2006JD007548, 2007. 26912

Emanuel, K. A. and Zivkovic-Rothman, M.: Development and evaluation of a convection scheme for use in climate models, J. Atmos. Sci., 56, 1766–1782, doi:10.1175/1520-0469(1999)056<1766:DAEOAC>2.0.CO;2, 1999. 26895, 26920

ACPD
13, 26893–26931, 2013

Emanuel, K. A., Neelin, J. D., and Bretherton, C. S.: On large-scale circulations in convecting atmospheres, Q. J. Roy. Meteor. Soc., 120, 1111–1143, doi:10.1002/qj.49712051902, 1994. 26896

Hack, J. J.: Parameterization of moist convection in the National Center for Atmospheric Research community climate model (CCM2), J. Geophys. Res.-Atmos., 99, 5551–5568, doi:10.1029/93JD03478, 1994. 26895, 26920

Hartmann, D. L. and Larson, K.: An important constraint on tropical cloud-climate feedback, Geophys. Res. Lett., 29, 1951, doi:10.1029/2002GL015835, 2002. 26909

Hartmann, D. L., Ockert-Bell, M. E., and Michelsen, M. L.: The effect of cloud type on Earths energy-balance – global analysis, J. Climate, 5, 1281–1304, doi:10.1175/1520-0442(1992)005<1281:TEOCTO>2.0.CO;2, 1992. 26895, 26907

Hartmann, D. L., Moy, L. A., and Fu, Q.: Tropical convection and the energy balance at the top of the atmosphere, J. Climate, 14, 4495–4511, doi:10.1175/1520-0442(2001)014<4495:TCATEB>2.0.CO;2, 2001. 26895

Hourdin, F., Musat, I., Bony, S., Braconnot, P., Codron, F., Dufresne, J. L., Fairhead, L., Filiberti, M. A., Friedlingstein, P., Grandpeix, J. Y., Krinner, G., Levan, P., Li, Z. X., and Lott, F.: The LMDZ4 general circulation model: climate performance and sensitivity to parametrized physics with emphasis on tropical convection, Clim. Dynam., 27, 787–813, doi:10.1007/s00382-006-0158-0, 2006. 26896

Jakob, C. and Siebesma, A. P.: A new subcloud model for mass-flux convection schemes: influence on triggering, updraft properties, and model climate, Mon. Weather Rev., 131, 2765–2778, doi:10.1175/1520-0493(2003)131<2765:ANSMFM>2.0.CO;2, 2003. 26902

Jacob, D. J., Prather, M. J., Rasch, P. J., Shia, R. L., Balkanski, Y. J., Beagley, S. R., Bergmann, D. J., Blackshear, W. T., Brown, M., Chiba, M., Chipperfield, M. P., deGrandpre, J., Dignon, J. E., Feichter, J., Genthon, C., Grose, W. L., Kasibhatla, P. S., Kohler, I., Kritz, M. A., Law, K., Penner, J. E., Ramonet, M., Reeves, C. E., Rotman, D. A., Stockwell, D. Z., Van-Velthoven, P. F. J., Verver, G., Wild, O., Yang, H., and Zimmermann, P.: Evaluation and intercomparison of global atmospheric transport models using Rn-222 and other short-lived tracers, J. Geophys. Res.-Atmos., 102, 5953–5970, doi:10.1029/96JD02955, 1997. 26905

Jöckel, P., Sander, R., Kerkweg, A., Tost, H., and Lelieveld, J.: Technical Note: The Modular Earth Submodel System (MESSy) – a new approach towards Earth System Modeling, Atmos. Chem. Phys., 5, 433–444, doi:10.5194/acp-5-433-2005, 2005. 26897

ACPD
13, 26893–26931, 2013

Jöckel, P., Kerkweg, A., Pozzer, A., Sander, R., Tost, H., Riede, H., Baumgaertner, A., Gromov, S., and Kern, B.: Development cycle 2 of the Modular Earth Submodel System (MESSy2), Geosci. Model Dev., 3, 717–752, doi:10.5194/gmd-3-717-2010, 2010. 26897

Johnson, R. H.: Partitioning tropical heat and moisture budgets into cumulus and mesoscale components – implications for cumulus parameterization, Mon. Weather Rev., 112, 1590–1601, doi:10.1175/1520-0493(1984)112<1590:PTHAMB>2.0.CO;2, 1984. 26900

Khairoutdinov, M., Randall, D., and DeMott, C.: Simulations of the atmospheric general circulation using a cloud-resolving model as a superparameterization of physical processes, J. Atmos. Sci., 62, 2136–2154, doi:10.1175/JAS3453.1, 2005. 26912

Klein, S. A. and Jakob, C.: Validation and sensitivities of frontal clouds simulated by the ECMWF model, Mon. Weather Rev., 127, 2514–2531, doi:10.1175/1520-0493(1999)127<2514:VASOFC>2.0.CO;2, 1999. 26908

Larson, K., Hartmann, D. L., and Klein, S. A.: The role of clouds, water vapor, circulation, and boundary layer structure in the sensitivity of the tropical climate, J. Climate, 12, 2359–2374, doi:10.1175/1520-0442(1999)012<2359:TROCWV>2.0.CO;2, 1999. 26896

Lohmann, U. and Roeckner, E.: Design and performance of a new cloud microphysics scheme developed for the ECHAM general circulation model, Clim. Dynam., 12, 557–572, doi:10.1007/s003820050128, 1996. 26910

Mahowald, N. M., Rasch, P. J., Eaton, B. E., Whittlestone, S., and Prinn, R. G.: Transport of (222)radon to the remote troposphere using the model of atmospheric transport and chemistry and assimilated winds from ECMWF and the National Center for Environmental Prediction NCAR, J. Geophys. Res.-Atmos., 102, 28139–28151, doi:10.1029/97JD02084, 1997. 26895, 26904

Nober, F. J. and Graf, H. F.: A new convective cloud field model based on principles of self-organisation, Atmos. Chem. Phys., 5, 2749–2759, doi:10.5194/acp-5-2749-2005, 2005. 26895

Nordeng, T. E.: Extended versions of the convective parametrization scheme at ECMWF and their impact on the mean and transient activity of the model in the tropics, Technical Momorandum 206, ECMWF Research Department, European Centre for Medium Range Weather Forecasts, Reading, UK, 1994. 26920

Pincus, R., Platnick, S., Ackerman, S. A., Hemler, R. S., and Patrick Hofmann, R. J.: Reconciling simulated and observed views of clouds: MODIS, ISCCP, and the limits of instrument simulators, J. Climate, 25, 4699–4720, doi:10.1175/JCLI-D-11-00267.1, 2012. 26930

ACPD
13, 26893–26931, 2013

Raisanen, P. and Jarvinen, H.: Impact of cloud and radiation scheme modifications on climate simulated by the ECHAM5 atmospheric GCM, Q. J. Roy. Meteor. Soc., 136, 1733–1752, doi:10.1002/qj.674, 2010. 26908

Randall, D., Khairoutdinov, M., Arakawa, A., and Grabowski, W.: Breaking the cloud parameterization deadlock, B. Am. Meteorol. Soc., 84, 1547–1564, doi:10.1175/BAMS-84-11-1547, 2003. 26895

Rasch, P. J., Feichter, J., Law, K., Mahowald, N., Penner, J., Benkovitz, C., Genthon, C., Giannakopoulos, C., Kasibhatla, P., Koch, D., Levy, H., Maki, T., Prather, M., Roberts, D. L., Roelofs, G. J., Stevenson, D., Stockwell, Z., Taguchi, S., Kritz, M., Chipperfield, M., Baldocchi, D., McMurry, P., Barrie, L., Balkansi, Y., Chatfield, R., Kjellstrom, E., Lawrence, M., Lee, H. N., Lelieveld, J., Noone, K. J., Seinfeld, J., Stenchikov, G., Schwartz, S., Walcek, C., and Williamson, D.: A comparison of scavenging and deposition processes in global models: results from the WCRP Cambridge Workshop of 1995, Tellus B, 52, 1025–1056, doi:10.1034/j.1600-0889.2000.00980.x, 2000. 26905

Ringer, M. A., McAvaney, B. J., Andronova, N., Buja, L. E., Esch, M., Ingram, W. J., Li, B., Quaas, J., Roeckner, E., Senior, C. A., Soden, B. J., Volodin, E. M., Webb, M. J., and Williams, K. D.: Global mean cloud feedbacks in idealized climate change experiments, Geophys. Res. Lett., 33, L07718, doi:10.1029/2005GL025370, 2006. 26896

Roeckner, E., Brokopf, R., Esch, M., Giorgetta, M., Hagemann, S., Kornblueh, L., Manzini, E., Schlese, U., and Schulzweida, U.: Sensitivity of simulated climate to horizontal and vertical resolution in the ECHAM5 atmosphere model, J. Climate, 19, 3771–3791, doi:10.1175/JCLI3824.1, 2006. 26897

Rossow, W. B. and Schiffer, R. A.: Advances in understanding clouds from ISCCP, B. Am. Meteorol. Soc., 80, 2261–2287, doi:10.1175/1520-0477(1999)080<2261:AIUCFI>2.0.CO;2, 1999. 26908, 26930

Soden, B. J. and Held, I. M.: An assessment of climate feedbacks in coupled ocean-atmosphere models (vol 19, pg 3354, 2006), J. Climate, 19, 6263–6263, doi:10.1175/JCLI9028.1, 2006. 26895, 26906

Solomon, S., Qin, M., Manning, M., Marquis, M., Averyt, K. B., Tignor, M., Miller, H. L., and Chen, Z.: Climate Change 2007: the Physical Science Basis: Contribution of Working Group I to the Fourth Assessment Report of the Intergovernmental Panel on Climate Change, Cambridge University Press, 2007. 26895

ACPD
13, 26893–26931, 2013

Stephens, G. L.: Cloud feedbacks in the climate system: a critical review, J. Climate, 18, 237–273, doi:10.1175/JCLI-3243.1, 2005. 26895

Tiedtke, M.: A comprehensive mass flux scheme for cumulus parameterization in large-scale models, Mon. Weather Rev., 117, 1779–1800, doi:10.1175/1520-0493(1989)117<1779:ACMFSF>2.0.CO;2, 1989. 26895, 26920

Tompkins, A. M.: A prognostic parameterization for the subgrid-scale variability of water vapor and clouds in large-scale models and its use to diagnose cloud cover, J. Atmos. Sci., 59, 1917–1942, doi:10.1175/1520-0469(2002)059<1917:APPFTS>2.0.CO;2, 2002. 26910

Tompkins, A., Bechtold, P., Beljaars, A., Benedetti, A., Cheinet, S., Janisková, M., Köhler, M., Lopez, P., and Morcrette, J.-J.: Moist Physical Processes in the IFS: Progress and Plans, Technical Memorandum 452, ECMWF, 2004. 26902

Tost, H., Jöckel, P., and Lelieveld, J.: Influence of different convection parameterisations in a GCM, Atmos. Chem. Phys., 6, 5475–5493, doi:10.5194/acp-6-5475-2006, 2006. 26895, 26896, 26897, 26904

Tost, H., Lawrence, M. G., Brühl, C., Jöckel, P., The GABRIEL Team, and The SCOUT-O3-DARWIN/ACTIVE Team: Uncertainties in atmospheric chemistry modelling due to convection parameterisations and subsequent scavenging, Atmos. Chem. Phys., 10, 1931–1951, doi:10.5194/acp-10-1931-2010, 2010. 26895, 26896, 26904

Turekian, K. K., Nozaki, Y., and Benninger, L. K.: Geochemistry of atmospheric radon and radon products, Annu. Rev. Earth Pl. Sc., 5, 227–255, doi:10.1146/annurev.ea.05.050177.001303, 1977. 26905

Webb, M., Senior, C., Bony, S., and Morcrette, J. J.: Combining ERBE and ISCCP data to assess clouds in the Hadley Centre, ECMWF and LMD atmospheric climate models, Clim. Dynam., 17, 905–922, doi:10.1007/s003820100157, 2001. 26908

Wilcox, E. M.: Spatial and temporal scales of precipitating tropical cloud systems in satellite imagery and the NCAR CCM3, J. Climate, 16, 3545–3559, doi:10.1175/1520-0442(2003)016<3545:SATSOP>2.0.CO;2, 2003. 26920

Wyant, M. C., Khairoutdinov, M., and Bretherton, C. S.: Climate sensitivity and cloud response of a GCM with a superparameterization, Geophys. Res. Lett., 33, L06714, doi:10.1029/2005GL025464, 2006. 26912

Yanai, M., Esbensen, S., and Chu, J. H.: Determination of bulk properties of tropical cloud clusters from large-scale heat and moisture budgets, J. Atmos. Sci., 30, 611–627, doi:10.1175/1520-0469(1973)030<0611:DOBPOT>2.0.CO;2, 1973. 26900

ACPD
13, 26893–26931, 2013

Zelinka, M. D. and Hartmann, D. L.: Why is longwave cloud feedback positive?, J. Geophys. Res.-Atmos., 115, D16117, doi:10.1029/2010JD013817, 2010. 26909

Zhang, G. J. and McFarlane, N. A.: Sensitivity of climate simulations to the parameterization of cumulus convection in the Canadian climate center general-circulation model, Atmos. Ocean, 33, 407–446, 1995. 26895, 26920

Zhang, K., Wan, H., Zhang, M., and Wang, B.: Evaluation of the atmospheric transport in a GCM using radon measurements: sensitivity to cumulus convection parameterization, Atmos. Chem. Phys., 8, 2811–2832, doi:10.5194/acp-8-2811-2008, 2008. 26895, 26904

Zhang, M. H., Lin, W. Y., Klein, S. A., Bacmeister, J. T., Bony, S., Cederwall, R. T., Del Genio, A. D., Hack, J. J., Loeb, N. G., Lohmann, U., Minnis, P., Musat, I., Pincus, R., Stier, P., Suarez, M. J., Webb, M. J., Wu, J. B., Xie, S. C., Yao, M. S., and Zhang, J. H.: Comparing clouds and their seasonal variations in 10 atmospheric general circulation models with satellite measurements, J. Geophys. Res.-Atmos., 110, D15S02, doi:10.1029/2004JD005021, 2005. 26908

ACPD

13, 26893–26931, 2013

Table 1. Convection parameterisations applied in the individual simulations; to differentiate between the reference-, 2 × CO_2-simulation and the two resolutions the following abbreviations are added to the simulation name: REF or 2 × CO_2 and T42 or T63.

Simulation name	Description
T1	Tiedtke scheme with modifications of Nordeng (Tiedtke, 1989; Nordeng, 1994)
EC	IFS cycle 29r1b from ECMWF (Bechtold et al., 2004)
EM	Emanuel and Zivkovic-Rothman (1999)
ZM	combined scheme of Zhang and McFarlane (1995) and Hack (1994) with a modification of Wilcox (2003)

ACPD
13, 26893–26931, 2013

Table 2. Calculated temperature increase ΔT and difference for the lowermost model layer (horizontally area weighted) with T1 as the reference simulation.

	T63		T42	
Simulation name	ΔT (K)	$\delta^i_{T1}(\Delta T)$ (K)	ΔT (K)	$\delta^i_{T1}(\Delta T)$ (K)
T1	3.4	–	3.3	–
EC	3.5	0.12	3.5	0.26
EM	3.3	−0.06	3.3	0.04
ZM	3.4	−0.03	3.4	0.07

ACPD
13, 26893–26931, 2013

Table 3. Change in globally averaged CRF as well as the change of the longwave and shortwave CRF component.

Simulation name	T63			T42		
	ΔCRF ($W m^{-2}$)	ΔCRF_{LW} ($W m^{-2}$)	ΔCRF_{SW} ($W m^{-2}$)	ΔCRF ($W m^{-2}$)	ΔCRF_{LW} ($W m^{-2}$)	ΔCRF_{SW} ($W m^{-2}$)
T1	1.09	−0.76	1.85	1.42	−0.70	2.12
EC	0.52	−0.04	0.56	0.24	0.11	0.13
EM	1.49	−0.36	1.85	2.00	−0.60	2.60
ZM	0.87	−0.20	1.07	1.27	−0.19	1.46

ACPD
13, 26893–26931, 2013

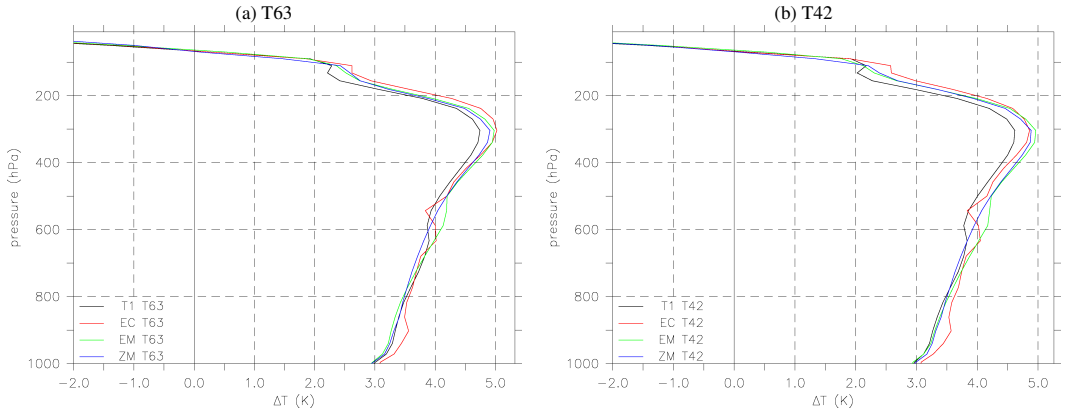

Fig. 1. Temperature difference ΔT of the global mean temperature profiles between the $2\times CO_2$- and REF-simulations for different convection parameterisations and two resolutions (left panel: T63; right panel: T42).

ACPD
13, 26893–26931, 2013

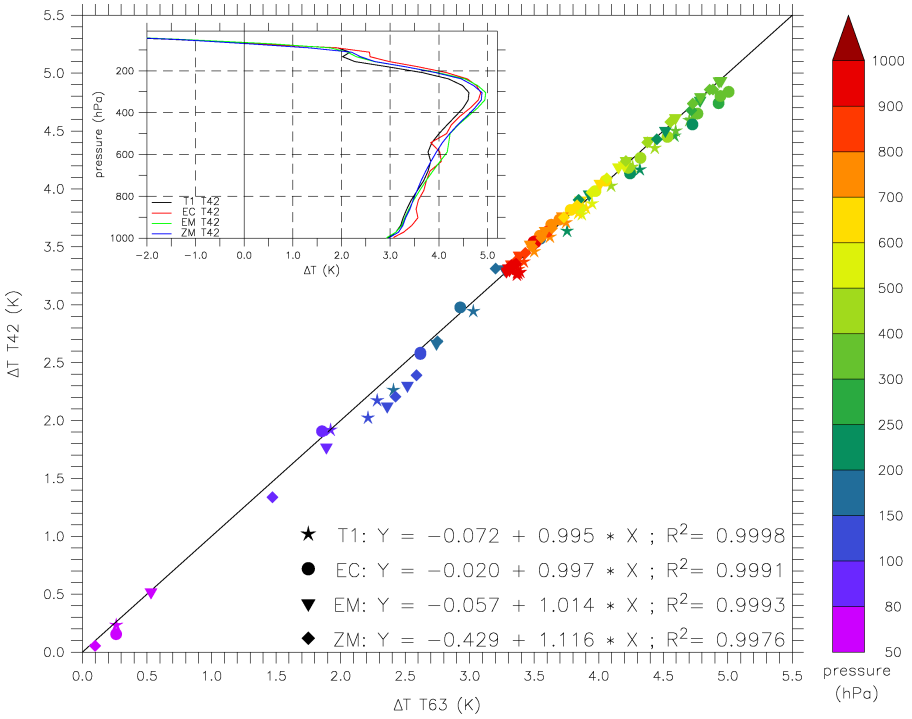

Fig. 2. Correlation of the temperature change ΔT between the resolutions T63 (horizontal axis) and T42 (vertical axis) for the individual simulations distinguished by symbols (T1 = star, EC = circle, EM = triangle and ZM = diamond) and colour coded with pressure altitude. The inner panel shows the temperature increase ΔT for the coarser resolution (T42), the same as Fig. 1b. The black line depicts the one-to-one correspondance.

ACPD
13, 26893–26931, 2013

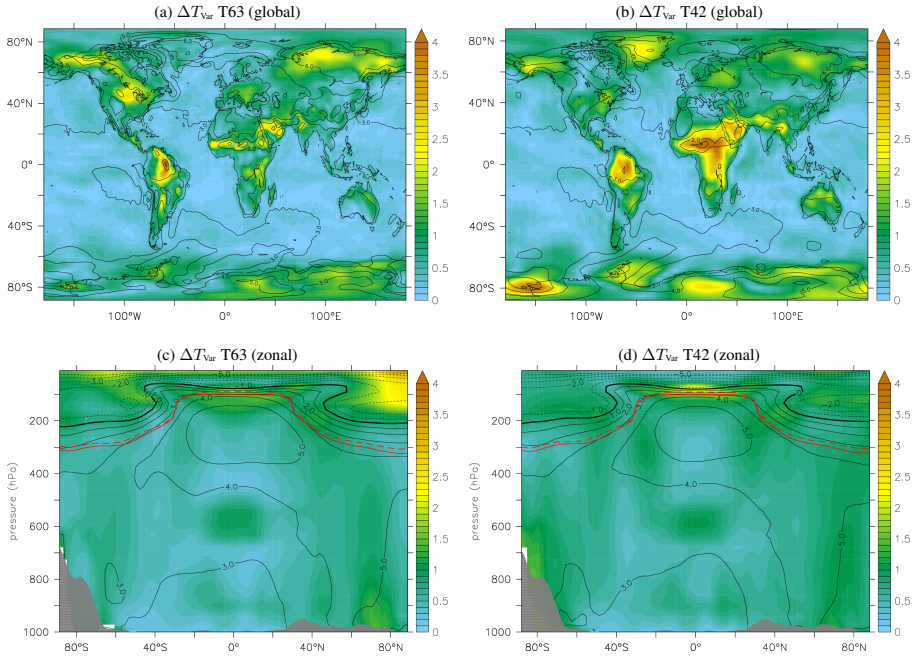

Fig. 3. Maximum error ΔT_{Var} of the temperature increase in Kelvin (colour coded); the upper panels illustrate regions of high variability for ΔT for the lowermost model layer, the lower panels show the same for the zonally averaged ΔT. The black contour lines denote the minimal temperature increase ΔT_{min} (see Eq. 4) with an interval of 1 K (black solid lines indicate positive and black dashed lines negative values). The red solid and dashed lines depict the averaged tropopause height for the reference- and 2 × CO_2-simulations, respectively.

ACPD
13, 26893–26931, 2013

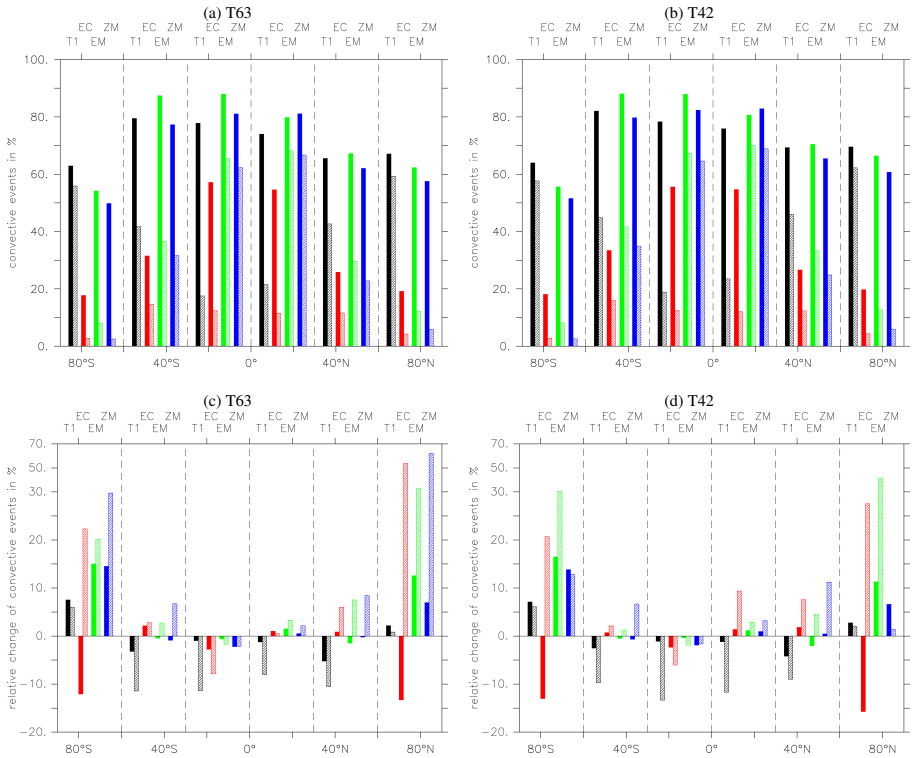

Fig. 4. Zonal average activation of the convection scheme in %. Each bar represents an average over 30° latitude (90 to 60° S, 60 to 30° S, etc.) for all simulations indicated in the top row of the graphs. The filled bars show the absolute activation of the convection parameterisation and the hatched bars count only deep convective events (and midlevel for T1 and EC). The two upper panels display the activation in the reference simulations and the lower ones the relative difference of the 2 × CO_2 against the REF-simulations.

ACPD
13, 26893–26931, 2013

Uncertainties in future climate predictions

H. Rybka and H. Tost

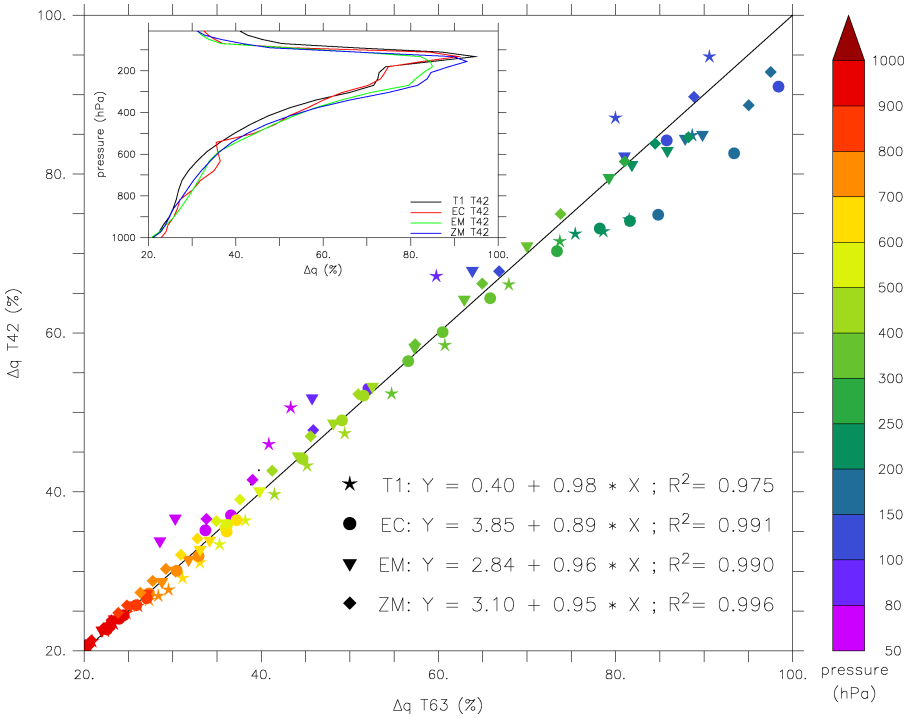

Fig. 5. Correlation of the change of specific humidity Δq in % between the resolutions T63 (horizontal axis) and T42 (vertical axis) for the individual simulations distinguished by symbols (T1 = star, EC = circle, EM = triangle and ZM = diamond) and colour coded with pressure altitude. The inner panel shows the increase in the specific humidity Δq in % for the coarser resolution (T42). The black line depicts the one-to-one correspondence.

ACPD
13, 26893–26931, 2013

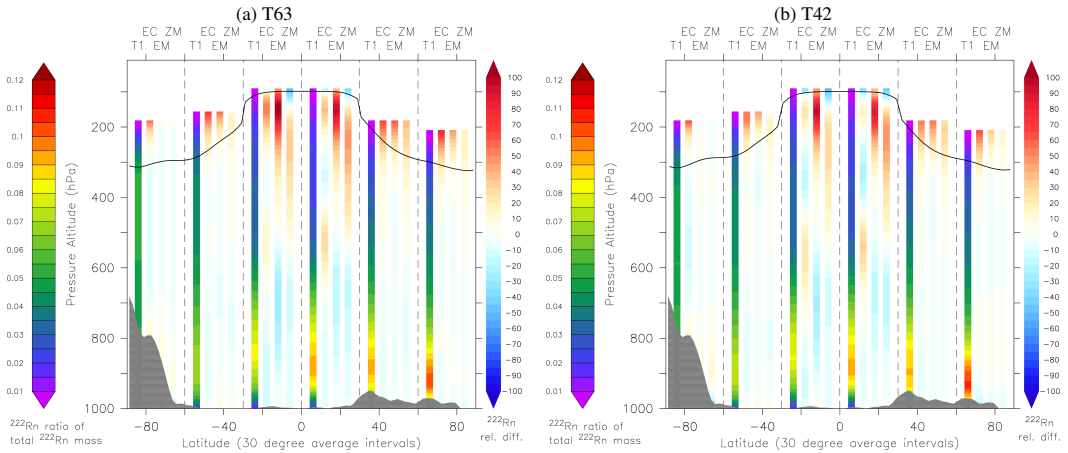

Fig. 6. Zonally averaged radon ratios of the total atmospheric radon mass. The vertical axis depicts the pressure altitude and each bar represents an average over 30° latitude (90 to 60° S, 60 to 30° S, etc.) for all simulations indicated in the top row of the graphs. The first bar in each bin shows the ratio for the T1 REF-simulations using the color bar on the left side. The other three bars in each bin indicate the relative difference in % to the Tiedtke simulations using the color scale on the ride hand side of the panel. The black solid line illustrate the mean tropopause height of the REF-simulations and the grey shaded area the zonal mean orography.

ACPD
13, 26893–26931, 2013

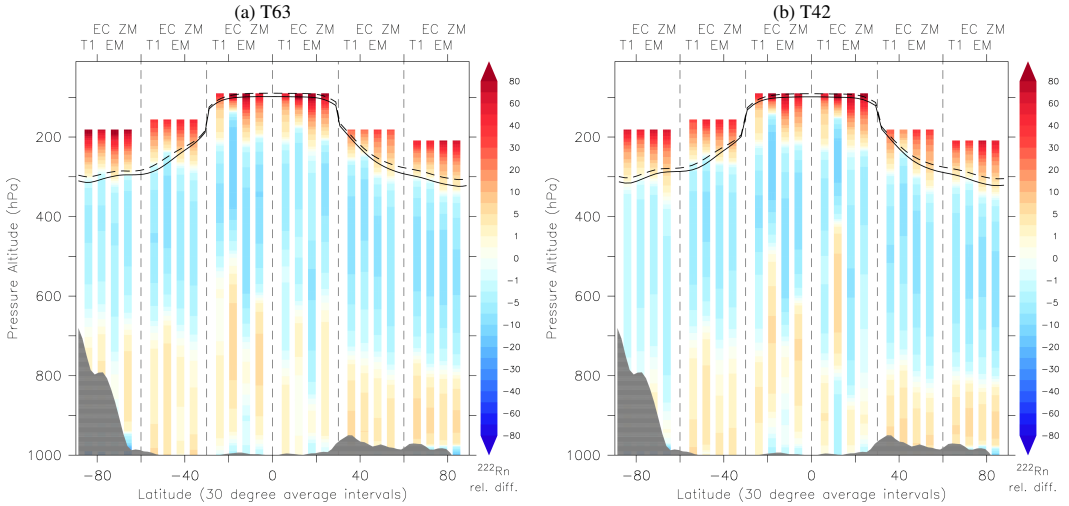

Fig. 7. Zonally averaged relative change in radon ratios in the 2 × CO_2-simulation. The vertical axis depicts the pressure altitude and each bar represents an average over 30° latitude (90 to 60° S, 60 to 30° S, etc.) for all simulations indicated in the top row of the graphs. The black solid (dashed) line illustrate the mean tropopause height of the REF- (2 × CO_2-) simulations and the grey shaded area the zonal mean orography.

ACPD
13, 26893–26931, 2013

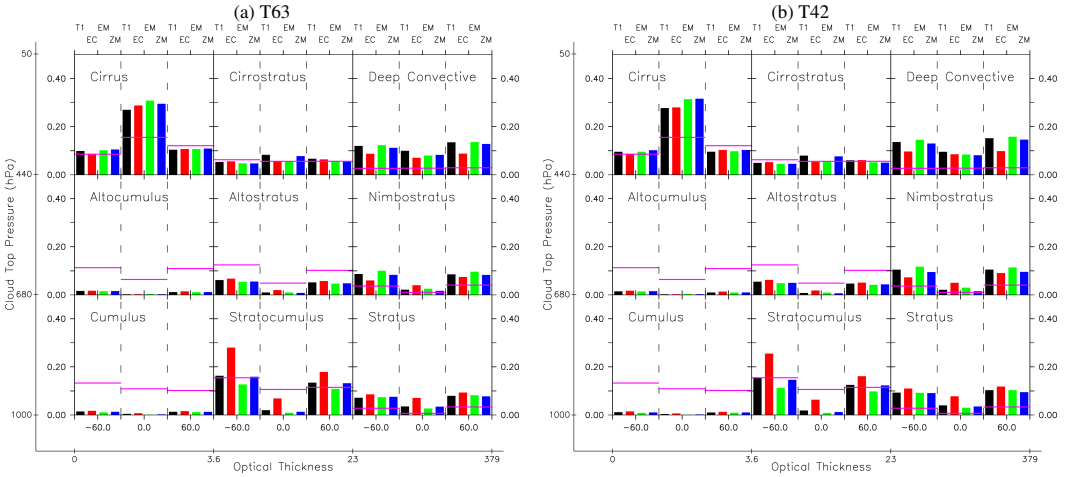

Fig. 8. Zonal average occurrence of various cloud types (unit: cloud amount per $\tau - p_c$ bin). Each bar represents an average over 60° latitude (90 to 30° S, etc.) for all REF-simulations indicated in the top row of the graphs. The purple horizontal lines show multi-year average values from 1984 until 2008 of the ISCCP D1 dataset (Pincus et al., 2012). The cloud type classification follows the ISCCP definitions by cloud top height and optical thickness (Rossow and Schiffer, 1999).

ACPD
13, 26893–26931, 2013

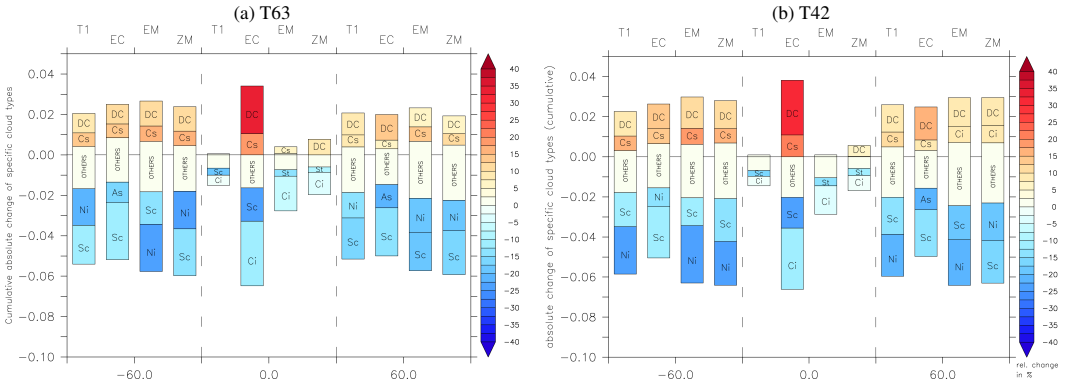

Fig. 9. Change of different cloud types in the 2 × CO_2-simulation. Each bar represents an average over 60° latitude (90 to 30° S, etc.) for all simulations indicated in the top row of the graphs. The *y* axis denote the absolute (cumulative) and the color bar the relative change in %. The height of one particular bar identifies the absolute increase/reduction of the corresponding cloud type. Only the two highest positive and negative changes are labelled with the following abbreviations: DC = Deep Convective, Cs = Cirrostratus, Sc = Stratocumulus, Ni = Nimbostratus, St = Stratus, As = Altostratus, Ci = Cirrus.

ACPD
13, 26893–26931, 2013